Opt Quant Electron (2008) 40:973–981
DOI 10.1007/s11082-009-9274-5

Design of type-II interband cascade lasers for terahertz emission

Khai Q. Le

Received: 11 March 2008 / Accepted: 30 January 2009 / Published online: 20 February 2009

Abstract We report the design of type-II interband cascade (IC) lasers emitting at terahertz (THz) range. The band structures are obtained using an eight-band $\mathbf{k} \cdot \mathbf{p}$ finite difference method with strain effects, which accounts for the coupling between the conduction and valence bands. Also, a detailed analysis of the interband transition energy in the type-II IC laser structures as a function of layer thickness is carried out using the self-consistent Schrödinger–Poisson calculations. The calculations show that the promising type-II IC lasers operating at 2.3 THz can be reached.

Keywords Interband cascade laser · Terahertz emission · $8 \times 8\,\mathbf{k} \cdot \mathbf{p}$ method

1 Introduction

Recently, the development of coherent-light sources in the terahertz (THz) frequency range has attracted a great deal of research interest due to the large number of possible application in bio-medical applications (Han et al. 2000), in atmospheric and astronomical spectroscopy (Mittleman 2002), in chemical monitoring and for the implementation of high-bandwidth intra-building wireless communications. Since the first demonstration of a quantum cascade (QC) laser in 1994 by Faist et al. (1994), a tremendous research effort has been devoted to extend the operating frequency in the far-infrared. QC lasers are unipolar semiconductor lasers that are based on intersubband transitions in a specifically engineered heterostructure. Contrary to conventional laser diodes, where the optical transition takes place across the band gap (interband) and thus involves both electrons and holes, in these novel devices only electrons are involved and the optical transition occurs between subbands belonging to the conduction band (intersubband). The working frequency can be tuned in a broad range by adjusting the width of the quantum wells and barriers, the material composition and

K. Q. Le (✉)
Department of Information Technology, Ghent University-IMEC, Sint-Pietersnieuwstraat 41, 9000 Ghent, Belgium
e-mail: ronaldokhai@yahoo.com

the applied bias. Recently, QC lasers have demonstrated laser operation at high power and far-infrared wavelengths as high as ∼143 μm (or 2.1 THz in frequency) and beyond (Williams et al. 2004; Ajili et al. 2004).

However, besides a great success in the wavelength range from mid-infrared to far-infrared with high power operating in pulsed mode as well as continuous-wave (CW) mode up to room temperature, QC lasers still suffer from relatively low radiative efficiencies due to a fast nonradiative relaxation between subbands via optical phonon scattering, which leads to substantial heating and high threshold current (Yang et al. 2002; Bradshaw et al. 2004; Yang et al. 2005). The aim to combine the advantage of an interband optical transition with interband tunneling to enable the cascading of type-II quantum well (QW) active regions (Meyer et al. 1995) as done in QC lasers can be attained using the novel approach of interband cascade (IC) lasers.

The concept of type-II IC lasers was first proposed in 1994 by Yang (1995) and demonstrated in 1997 by Lin et al. (1997). Using an interband tunneling facilitated by the broken band-gap alignment in type-II QWs, IC lasers reuse injected electrons and form cascaded interband transitions for multiple photon generation, leading to a quantum efficiency significantly greater than QC lasers. In addition, using optical transitions between conduction and valence bands with opposite dispersion curvatures, IC lasers circumvent the fast phonon scattering loss in intersubband QC lasers and possess a wide wavelength tailoring range from mid-infrared to far-infrared. However, to our best knowledge, lack of report on type-II IC lasers operating at THz range has been published in the open literatures so far.

In this work, we report the design of type-II IC lasers, which are promising for ∼87–130 μm emission wavelength (or 2.3–3.5 THz in frequency). The band structure is determined using the eight-band $\mathbf{k} \cdot \mathbf{p}$ finite difference method within the framework of the self-consistent Schrödinger–Poisson solution (Liu and Chuang 2002).

2 Design method

2.1 Basic theory of interband transition in type-II IC lasers

The concentration of the IC laser structure design is to optimize the active region. In this work, the active region design is based on the interband transition and interband tunneling in InAs/InGaSb/AlSb type-II QWs, which includes the processes of injector, laser emission, tunneling, transfer and recycling as clearly seen in Fig. 1 (Meyer et al. 2006). From this structure, the discrete energy levels including the first energy level (E_{C1}) in the InAs QW in the conduction band, the topmost energy level in the InGaSb QW in the valence band (E_{HH1}-heavy hole 1) and the topmost energy level in GaSb QW in the valence band (E_{HH2}-heavy hole 2) are made due to quantum confinement in the QWs. Under a forward bias, electrons injected from an injection region into the energy level E_{C1} make radiative transition from E_{C1} to E_{HH1}, which corresponds to the desired emission wavelength. Subsequently, electrons at state E_{HH1} can cross the thin AlSb barrier and GaSb layer by tunneling and scattering into the conduction band of the next injection region because of a strong spatial interband coupling (a unique feature of type-II heterostructure) (Yang et al. 1997) and are ready for the next interband transition, which leads to sequential photon generation.

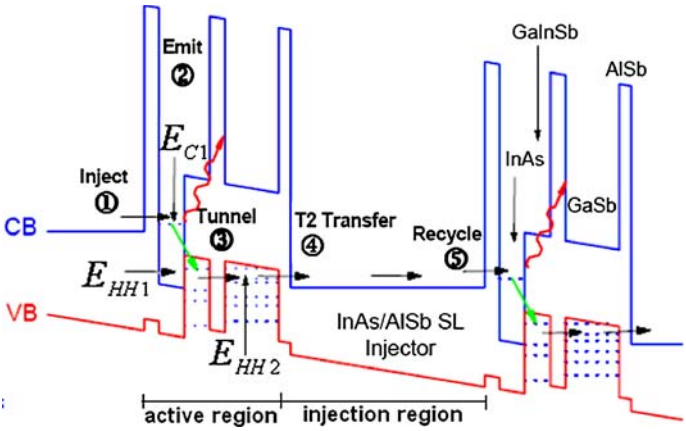

Fig. 1 Interband cascade structure based on InAs/InGaSb/AlSb type-II QWs

2.2 Band structure calculation

Within the envelope function approximation (EFA) and the eight-band $\mathbf{k} \cdot \mathbf{p}$ model with the inclusion of the coupling of the conduction and valence bands (Liu and Chuang 2002), the eigenstates of the IC structures are obtained by solving the Schrödinger equation

$$H_{8\times8}\Psi(z, k_t) = E_m(k_t)\Psi(z, k_t), \tag{1}$$

where $\Psi(z, k_t)$ is the total carrier wave function, $E_m(k_t)$ is the subband energy with index m, k_t is the in-plane wave vector and $H_{8\times8}$ is the Hamiltonian. Under axial approximation, the Hamiltonian $H_{8\times8}$ can be transformed into two 4×4 blocks diagonalized Hamiltonian. The Hamiltonian matrices can be found for lattice-mismatched biaxially strained bulk semiconductors without external perturbation (Liu and Chuang 2002). With the spin degeneracy taken into account, the eight-band $k \cdot p$ model reduces to a four-band model including the conduction band (C), the heavy-hole (HH), the light-hole (LH), and the spin-orbit split-off (so) band.

For a quantum well, the carrier wave function can be written as

$$\Psi_m(z, k_t) = \frac{e^{ik_t r}}{\sqrt{A}} \sum_{i=1}^{4} g_m^i(z) \left|u_i\right\rangle, \tag{2}$$

where A is the area of the QW, $r = \sqrt{x^2 + y^2}$, $g_m^i(z)$ is the carrier envelope function, and $|u_i\rangle$ is the basis function. The carrier wave functions and subband energies, which can be either the conduction or the valence band, can be determined by solving four coupled effective mass equations

$$\sum_{j=1}^{4} H_{4\times4,ij}(k_t, k_z) g_m^j(z) = E_m(k_t) g_m^j(z), \quad \text{for } i = 1, 2, 3, 4. \tag{3}$$

In this work, the coupled differential Eq. 3 is solved using the finite difference method. Note that during the numerical code implementation, the results will include some spurious solutions for subband energies due to the solutions outside of the first Brillouin zone (Szmulowicz 2005). Extra care is needed to select the proper eigenvalues for the energies.

2.3 Self-consistent solution for type-II quantum wells

The presence of an external potential and carrier distribution of the electrons and holes from dopants confined separately in different layers in type-II QW structure based on Antimonide material (Sb) causes an electric screening field, resulting in a band bending and energy shifting. These effects strongly change the electronic band structure of the QW. Therefore we need a self-consistent approach that takes into account of the carrier screening effects. For a QW of width L_z grown along the [001] direction, the total potential energies $V_c(z)$ and $V_v(z)$ for each band are sums of the built-in QW potential and the screening potential profiles

$$V_c(z) = V_{cw}(z) - |e|\,\phi(z) \tag{4}$$

$$V_v(z) = V_{vw}(z) - |e|\,\phi(z) \tag{5}$$

where $V_{cw}(z)$ and $V_{vw}(z)$ are the built-in QW potentials for the conduction and valence band, respectively, and $\phi(z)$ is the screened electrostatic potential induced by charge carriers in the QW, which satisfies Poisson's equation

$$\frac{\mathrm{d}}{\mathrm{d}z}\varepsilon(z)\frac{\mathrm{d}\phi}{\mathrm{d}z} = -|e|\,[p(z) - n(z) + N_D(z) - N_A(z)] \tag{6}$$

where $\varepsilon(z)$ is the permittivity of the well (or barrier), $p(z)$ and $n(z)$ are the charge densities of holes and electrons, respectively, and $N_D(z)$ and $N_A(z)$ are the densities of ionized donors and acceptors, respectively ($N_D = N_A = 0$ in this work since the active layers are undoped). The charge densities $p(z)$ and $n(z)$ are given by

$$n(z) = \frac{1}{A}\sum_m \sum_{k_t} |\Psi_m(z, k_t)|^2 f_m(k_t), \tag{7}$$

$$p(z) = \frac{1}{A}\sum_n \sum_{k_t} |\Psi_n(z, k_t)|^2 [1 - f_n(k_t)], \tag{8}$$

where A is the area of the active region, m denotes the mth conduction subband and n denotes the nth valence subband, f_m and f_n are the Fermi functions for the mth subband in conduction band and the nth subband in the valence band, and $\Psi_m(z, k_t)$ and $\Psi_n(z, k_t)$ are the conduction and valence band envelope functions, respectively. The summation over m (or n) represents the summation over all eigenstates. In this work, only energy levels in bound-state are taken into account. The Fermi energy levels are determined by equilibrium conditions given by

$$N = \int_0^\infty n(z)\mathrm{d}z = \int_0^\infty p(z)\mathrm{d}z, \tag{9}$$

where N is doping concentration in systems. The Eqs. 7 and 8 can be solved using the Newton method. The Schrödinger equation (3) and the Poisson equation (6) are solved numerically until a self-consistent solution with free-carrier screening of the electric field is obtained.

3 Numerical results and discussion

In order to verify our developed code for band structure calculations in type-II IC laser structures, we have performed some calculations based on the eight-band $\mathbf{k}\cdot\mathbf{p}$ finite difference method and compared them with experimental and numerical results reported in the literatures. We replicate the band structure of mid-IR type-II IC lasers in Liu and Chuang (2002).

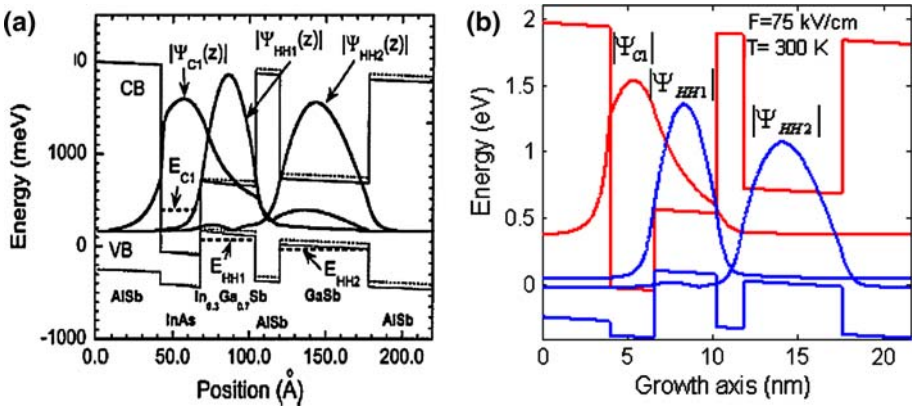

Fig. 2 Schematic band structure diagram of a portion of type-II IC laser under applied bias at T = 300 K created by Liu and Chuang (2002) (**a**) and our calculation (**b**). The *solid curves* present the modulus of the wave functions for the first conduction subband and two topmost valence subbands at zone center

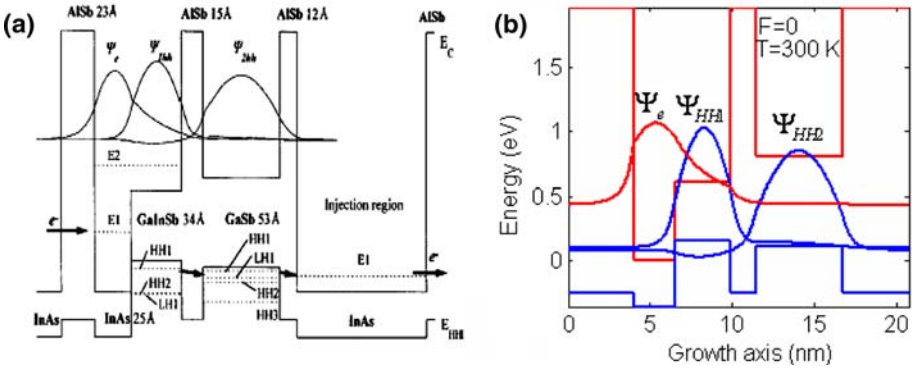

Fig. 3 Schematic band structure diagram of a portion of type-II IC laser without applied bias at T = 300 K created by Yang et al. (1998) (**a**) and our calculation (**b**). The *solid curves* present the wave functions for the first conduction subband and two topmost valence subbands at zone center

The parameters used for calculations are the same as their work. For the type-II IC laser structure under applied bias of F = 75 kV/cm in Liu and Chuang (2002), the calculated interband transition energy of 323.9 meV (or 3.83 μm in wavelength) between the first conduction band (C1) and the first valence band (heavy hole, HH1) edge energies at the zone center have been reported. The measured result in Mu and Yang (1999) is 322 meV (or 3.85 μm in wavelength) while our calculated result is 324.3 meV (or 3.82 μm in wavelength). It can be clearly seen that our calculated result is in good agreement with the published calculation and measured result. The wave functions of the first conduction subband and two topmost valence subbands with and without (Yang et al. 1998) an applied electric field at 300 K are depicted in Figs. 2 and 3 while the energy band structure with respect to in-plane wave vector ($\boldsymbol{k}$) under applied bias is presented in Fig. 4.

For the W-shaped IC laser structure in Liu and Chuang (2002), the published calculation result of energy separation between the first two conduction subbands (C1 and C2) is 152 meV while our calculated result is exactly 152.4 meV. The relevant wave functions of the first two conduction subbands and the first two valence subbands are presented in Fig. 5.

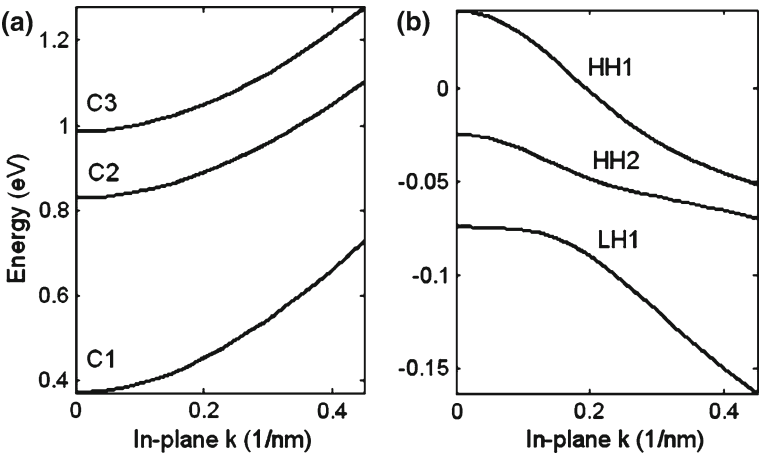

Fig. 4 The calculated energy dispersion curves are plotted for three conduction subbands (**a**) and three topmost valence subbands (**b**) at T = 300 K

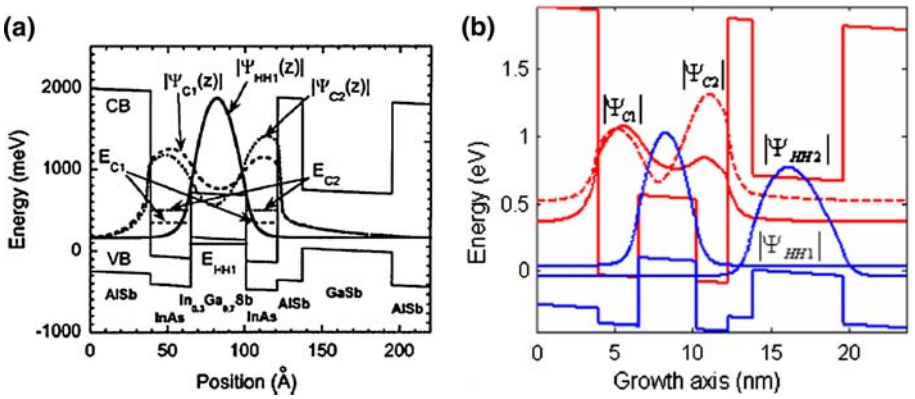

Fig. 5 Schematic band structure diagram of a portion of W-shaped type-II IC laser under applied bias at T = 300 K created by Liu and Chuang (2002) (**a**) and our calculation (**b**). The *solid curves* present the modulus of the wave functions for two first conduction subbands and the topmost valence subband at zone center

The comparisons of our calculated results with the published results establish the reliability of our numerical code implementation.

With our confident numerical code, we now pay attention on the design of type-II IC lasers for THz emission. The IC laser structure is based on the interband cascade scheme as shown in Fig. 1. Note that whenever we carry out the design of type-II IC laser structures, they have to satisfy the energy staircase to enable sequential photon generation. The relevant wave functions of two successive energy levels involved in the electron transfer processes should be overlapped. In addition, one of the most important points in THz IC laser design one should pay attention on is the temperature performance of the proposed structure. However, the theoretical evaluation of the temperature performance of the device is now suffering from

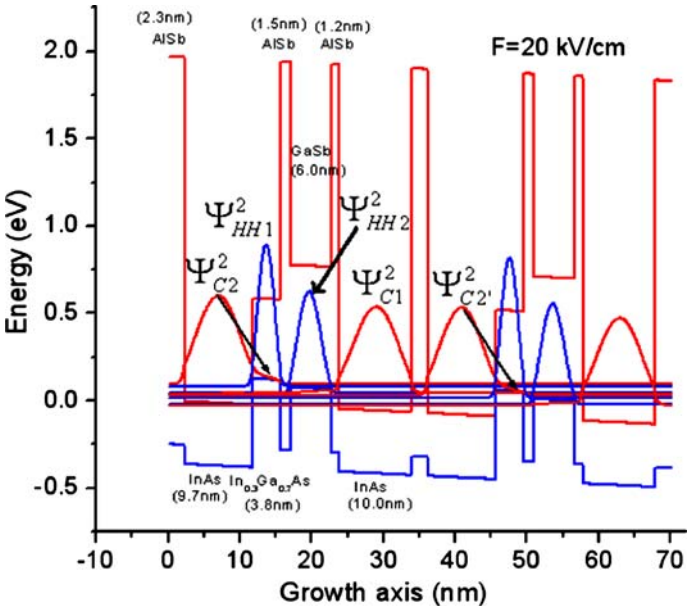

Fig. 6 Conduction and valence bands profiles for two period of type-II IC laser, the moduli squared of the relevant wave functions of the conduction and valence subbands under applied bias F = 20 kV/cm

the fact that there is lack of an efficient theoretical model. Therefore, we do not address it in this work.

By tailoring the thickness of certain quantum wells and barriers, we found that under electric field of F = 20 kV/cm, one period of IC laser structure made of 2.3 nm AlSb, 9.7 nm InAs, 3.8 nm InGaSb, 1.5 nm AlSb, 6.0 nm GaSb, and 1.2 nm AlSb undoped-layers, and 10 nm InAs injection doped-layer can be generated the emission wavelength at ∼130 μm (or 2.3 THz in frequency). The electronic band structure diagram is depicted in Fig. 6 whilst the energy band structure with respect to in-plane wave vector is presented in Fig. 7. Moreover, a wider or thinner InAs QW in the active core leads to the freedom in reduction or enlargement of the separation between the upper lasing level (E_{C1}) and the lower lasing level (E_{HH1}), which is promising for 2.3−3.5 THz IC laser design.

It is important for IC laser design to investigate the dependence of transition energy on the layer thickness. Let us now examine how the width of InAs and InGasSb QWs in the active region affects on the subbands, separation energy between the first conduction subband in the injector well (C1) and the first conduction subband in the active well of the next stage (C2′) and transition energy of the IC laser structure. The subbands, energy separation between C1 and C2′ and transition energy of the IC laser structure calculated as function of the thickness of InAs layer (93–97Å) is presented in Fig. 8a. As can be seen from the figure, as the width of InAs QW increases, the E_{C1} gradually decreases from 96.7 to 90.6 mev while E_{HH1} slightly decreases from 82.3 to 81 meV. It leads the transition energy gradually decrease from 14.4 meV (3.5 THz) to 9.6 meV (2.3 THz) while the separation energy gradually increases from 11.5 to 17.8 meV. The topmost curve shows that E_{C1} falls with the width of InAs QW, supporting the notion that the larger the well width, the lower the confined energy is. It is obviously that by tailoring the width of InAs QW, the desired emission wavelength at ∼130 μm (or 2.3 THz in frequency) can be reached while the cascading scheme is still remained. Also,

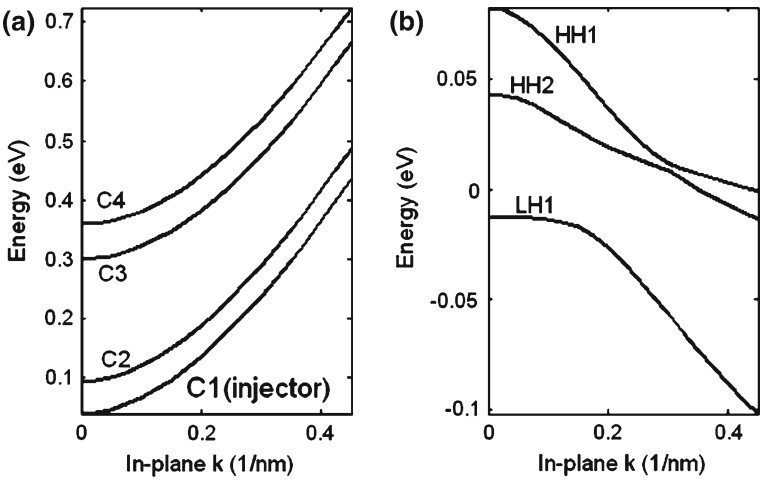

Fig. 7 The calculated energy dispersion curves are plotted for four conduction subbands (**a**) and three topmost valence subbands (**b**) at T = 300 K

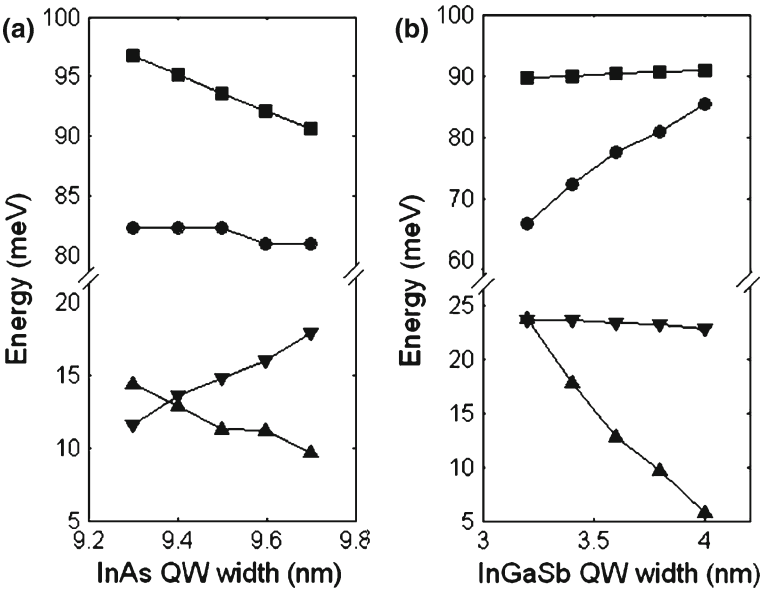

Fig. 8 Dependence of conduction subband C1 (*black square*), valence subband HH1 (*bullet*), separation energy between C1 and C2′ (*black triangle down*) and transition energy (*black triangle*) on the InAs QW width (**a**) and InGaSb QW width (**b**)

the subbands, energy separation between C1 and C2′ and transition energy of the IC laser structure calculated as function of the thickness of InGaSb QW (32−40 Å) are depicted in Fig. 8b. As sketched in the figure, as InGaSb QW widens and InAs QW is fixed at 9.7 nm, E_{HH1} gradually increases while E_{C1} is slightly fixed. It leads the transition energy drops quickly while the separation energy between C1 and C2′ slightly decreases. It is clearly seen that the width of InAs and InGaSb QWs strongly impact on the transition energy in the IC

laser structures. By carefully tailoring their thickness, the desired emission wavelength is attained.

4 Conclusions

In summary we have presented the calculation and design of the type-II IC laser structure using the eight-band $\mathbf{k} \cdot \mathbf{p}$ finite difference method within the framework of the self-consistent Schrödinger–Poisson solution. This structure is very promising for the production of type-II IC lasers operating at 2.3–3.5 THz. Also, the dependence of conduction and valence subbands and interband transition energy on the layer thickness has been investigated. This work is useful for the design of the terahertz light emission based on type-II IC lasers.

References

Ajili, L., Scalari, G., Faist, J., Beere, H., Linfield, E., Ritchie, D., Davies, G.: High power quantum cascade lasers operating at (lambda) 87 μm and 130 μm. Appl. Phys. Lett. **85**, 3986–3988 (2004). doi:10.1063/1.1810217

Bradshaw, J.L., Breznay, N.P., Bruno, J.D., Gomes, J.M., Pham, J.T., Towner, R.J., Wortman, D.E., Tober, R.L., Monroy, C.J., Olver, K.A.: Recent progress in the development of type II interband cascade lasers. Physica E **20**, 479–485 (2004). doi:10.1016/j.physe.2003.08.063

Faist, J., Capasso, F., Sivco, D.L., Hutchinson, A.L., Cho, A.Y.: Quantum cascade laser. Science **64**, 553–556 (1994). doi:10.1126/science.264.5158.553

Han, P.Y., Cho, G.C., Zhang, X.C.: Time-domain transillumination of biological tissues with terahertz pulses. Opt. Lett. **25**, 242–244 (2000). doi:10.1364/OL.25.000242

Lin, C.H., Yang, R.Q., Zhang, D., Murry, S.J., Pei, S.S., Allerman, A.A., Kurtz, S.R.: Type-II interband quantum cascade laser at 3.8 μm. Electron. Lett. **33**, 597–598 (1997). doi:10.1049/el:19970421

Liu, G., Chuang, S.L.: Modelling of Sb-based type-II quantum cascade lasers. Phys. Rev. B. **65**, 165220–165229 (2002). doi:10.1103/PhysRevB.65.165220

Meyer, J.R., Hoffman, C.A., Bartoli, F.J., Ram-Mohan, L.R.: Type-II quantum-well lasers for the mid-wavelength infrared. Appl. Phys. Lett. **67**, 757–759 (1995). doi:10.1063/1.115216

Meyer, J.R., Canedy, C.L., Kim, C.S., Kim, M., Bewley, W.W., Vurgarftman, I., Lindle, J.R., Larrabee, D.C., Nolde, J.A.: The 2nd International workshop on quantum cascade laser, 6th–9th September 2006, Brindisi, Italy

Mittleman, D.M.: Sensing with Terahertz Radiation. Springer, Berlin (2002)

Mu, Y.M., Yang, R.Q.: Modeling of InAs/GaInSb/AlSb type-II mid-IR interband cascade lasers. Proc. SPIE. **3625**, 881 (1999)

Szmulowicz, F.: Solution to spurious bands and spurious real solutions in the envelope-function approximation. Phys. Rev. B **71**, 245117–245129 (2005). doi:10.1103/PhysRevB.71.245117

Williams, B.J., Kumar, S., Hu, Q., Reno, J.L.: Resonant-phonon terahertz quantum cascade laser operating at 2.1 THz ($\lambda = 141$ μm). Electron. Lett. **40**, 431–433 (2004). doi:10.1049/el:20040300

Yang, R.Q.: Infrared laser based on intersubband transitions in quantum wells. Superlattices Microstruct. **77**, 77–83 (1995). doi:10.1006/spmi.1995.1017

Yang, R.Q., Yang, B.H., Zhang, D., Lin, C.H., Murry, S.J., Wu, H., Pei, S.S.: High power mid-infrared interband cascade lasers based on type-II quantum wells. Appl. Phys. Lett. **71**, 2409–2411 (1997). doi:10.1063/1.120076

Yang, B.H., Zhang, D., Yang, R.Q., Lin, C.H., Murry, S.J., Pei, S.S.: Mid-infrared interband cascade lasers with quantum efficiencies >200%. Appl. Phys. Lett. **72**, 2220–2222 (1998). doi:10.1063/1.121265

Yang, R.Q., Bradshaw, J.L., Bruno, J.D., Pham, J.T., Wortman, D.E.: Mid-infrared type-II interband cascade lasers. IEEE J. Quantum Electron. **38**, 559–568 (2002). doi:10.1109/JQE.2002.1005406

Yang, R.Q., Hill, C.J., Yang, B.H.: High-temperature and low-threshold midinfrared interband cascade lasers. Appl. Phys. Lett. **87**, 151109–151111 (2005). doi:10.1063/1.2103387